HHS Public Access

Author manuscript

Nat Nanotechnol. Author manuscript; available in PMC 2018 June 04.

Published in final edited form as:

Nat Nanotechnol. 2018 January ; 13(1): 72–81. doi:10.1038/s41565-017-0009-7.

Synthetically Lethal Nanoparticles for Treatment of Endometrial Cancer

Kareem Ebeid[1], **Xiangbing Meng**[2,3], **Kristina W Thiel**[2], **Anh-Vu Do**[1], **Sean M Geary**[1], **Angie S Morris**[1], **Erica L Pham**[1], **Amaraporn Wongrakpanich**[1,4], **Yashpal S Chhonker**[5], **Daryl J Murry**[1,5], **Kimberly K Leslie**[2,3], and **Aliasger K Salem**[1,3]

[1]Division of Pharmaceutics and Translational Therapeutics, College of Pharmacy, University of Iowa, Iowa City, IA 52242, USA [2]Department of Obstetrics and Gynecology, University of Iowa, Iowa City, IA 52242, USA [3]Holden Comprehensive Cancer Center, University of Iowa, Iowa City, IA 52242, USA [4]Department of Pharmacy, Faculty of Pharmacy, Mahidol University, Bangkok, 10400, Thailand [5]Department of Pharmacy Practice, College of Pharmacy, University of Nebraska Medical Center, Omaha, NE 68198, USA

Abstract

Uterine serous carcinoma, one of the most aggressive types of endometrial cancer, is characterized by poor outcomes and mutations in the tumor suppressor p53. Our objective was to engender synthetic lethality to paclitaxel, the frontline treatment for endometrial cancer, in tumors with mutant p53 and enhance therapeutic efficacy using polymeric nanoparticles. First we identified the optimal nanoparticle formulation through comprehensive analyses of release profiles, cellular uptake and cell viability studies. Not only were paclitaxel-loaded nanoparticles superior to paclitaxel in solution, but the combination of paclitaxel-loaded nanoparticles with the antiangiogenic molecular inhibitor, BIBF-1120, promoted synthetic lethality specifically in cells with loss of function p53 mutation. In a xenograft model of endometrial cancer, this combinatorial therapy resulted in marked inhibition of tumor progression and extended survival. Together, our data provide compelling evidence for future studies of BIBF-1120- and paclitaxel-loaded nanoparticles as a therapeutic opportunity for loss of function p53 cancers.

Endometrial cancer (EC) is the most prevalent gynecological malignancy in the USA[1], with incidence and mortality on the rise due in large part to the obesity epidemic[1]. Importantly, EC is one of only two common cancers defying the general trend of improvement in incidence and mortality, with survival worse today than in the 1970s[1]. EC is classified into two major subtypes based on clinicopathological properties[2]. Type I EC is well

Correspondence to: Kimberly K Leslie; Aliasger K Salem.

Author contributions

K.E., X.M., K.K.L., and A.K.S. conceived and designed the experiments. K.E., X.M., S.M.G., A.D., A.S.M., E.L.P., A.W., Y.S.C., and D.J.M. performed the experiments. K.E., K.W.T., K.K.L. and A.K.S. wrote and revised the manuscript.

Competing financial interests

KWT is a co-founder of Immortagen, Inc. All other authors declare no competing financial interests.

differentiated, typically detected at an early stage, represents 80% of all cases and is associated with a favorable prognosis[2]. In contrast, the poorly differentiated type II EC includes mainly uterine serous carcinomas (USC) and portends poor prognosis[2]. Though USC represents only 10% of all EC cases, it contributes to 39% of total EC deaths[3]. The mainstay therapy for USC is chemotherapy and/or radiotherapy, a standard that has been in place for over two decades[4]. While numerous clinical trials have explored molecular inhibitors as monotherapies, they have generally failed to improve survival, suggesting that combinatorial therapies that rationally pair molecular inhibitors with standard chemotherapy may improve outcomes[5].

Mutations in *TP53* (the gene that encodes p53) occur in over 90% of USC[6] and are of three basic functional classes: (1) truncating, frameshift or splice site loss of function (LOF) mutations that result in protein instability and a p53-null state, (2) missense mutations that often result in gain of oncogenic function (GOF), and (3) synonymous/silent mutations that are wild-type (WT) equivalent[7].

As the guardian of the genome, p53 controls cycle checkpoints to allow cells to repair damaged DNA or induce apoptosis[8]. Activation of cell cycle checkpoints prevents progression into vulnerable phases of the cell cycle during treatment with chemotherapy. For example, paclitaxel (PTX) kills dividing cells in mitosis (M) through stabilizing mitotic-spindle microtubules[9]. Enforcing the G2/M checkpoint allows tumor cells to repair DNA before entering M, leading to chemoresistance[10,11]. In addition to p53, emerging data suggest that p38MAPK can also maintain the G2/M checkpoint[12,13]. In cells with LOF p53, p38 is activated as an alternative means to maintain the G2/M checkpoint[14].

Our group established that the combination of PTX with tyrosine kinase inhibitors (TKI) induces synergistic cell death specifically in LOF p53 cancer cells due to abrogation of the G2/M checkpoint[15,16]. Cells arrest in M and die due to mitotic catastrophe[15,16]. This phenomenon is termed synthetic lethality, a historical genetic observation that in the presence of certain single gene mutations, blocking or mutating a second gene leads to cell death, though neither mutation alone has a phenotype[17]. The concept of synthetic lethality has been explored in several clinical contexts, and the most successful to date is the use of poly (ADP-ribose) polymerase inhibitors in tumors with mutations in *BRCA*[18,19]. With respect to synergistic cell death from combining PTX and TKI, synthetic lethality means capitalizing on the presence of a p53 mutation to block the compensatory survival pathways activated as a result of the mutation. This approach is a novel application of synthetic lethality for p53 mutations given that the majority of studies have attempted to restore wild-type function[20]. The advantage of this approach is that it adds a degree of cancer targeting as this combination will pose specific cytotoxicity only in cancer cells with a LOF p53 mutation, sparing the normal cells that do not carry the mutation.

Building on our previous work, herein we have developed an innovative approach to significantly enhance the efficacy of PTX+TKI combinatorial treatment for USC.

First, we explored the use of a triple angiokinase molecular inhibitor, BIBF-1120 (BIBF, also known as nintedanib), that inhibits multiple tyrosine kinase receptors (vascular

endothelial growth factor receptors, platelet derived growth factor receptors and fibroblast growth factor receptors (FGFR)[21]) and induces cell death when combined with PTX in USC cells[16]. Two phase III trials in ovarian and non-small cell lung cancer (NSCLC) demonstrated significantly improved survival when BIBF was combined with chemotherapy[22,23]. However, adverse gastrointestinal events were increased in the groups that received nintedanib, indicating that additional strategies to improve the safety of the combinatorial strategy are necessary.

Second, we developed a polymeric nanoparticle (NP) delivery system to improve efficacy and safety of the combinatorial strategy. NP are well-established to: 1) enhance dissolution, which overcomes the reported low water solubility of PTX and BIBF, 2) improve pharmacokinetics, 3) minimize side effects due to decreased off-target effects, and 4) passively target tumors through the enhanced permeability and retention effect (EPR)[24]. This is a phenomenon observed in solid tumors, where excessive angiogenic signals result in the formation of defective "leaky" tumor vasculature, through which NP <200 nm in size can extravasate to the tumor microenvironment. The increased tumor mass also leads to ineffective lymphatic drainage, which subsequently increases NP retention[25]. Finally, we investigated the impact of varying NP formulations on major physicochemical properties of the prepared NP, drug loading, cytotoxicity, cellular uptake and drug release.

1 Synthetic lethality to soluble BIBF+PTX in LOF p53 cells

We first investigated the involvement of p53 mutational status on the sensitivity of EC cell lines to the combination of BIBF and PTX. Three different EC cell lines bearing different p53 mutations were utilized in the study: Ishikawa cells (WT p53), Hec50co cells (LOF p53 mutation that results in a p53-null status) and KLE cells (GOF p53 due to R175H mutation). These cells are all wild-type for the BIBF target, FGFR2 (Figure S1). Cells were incubated with soluble PTX (PTX**s**) or soluble BIBF (BIBF**s**) or the combination. Analysis of cell viability revealed that only Hec50co cells with LOF p53 were sensitive to the combination (Fig. 1a), with a three-fold decrease in viability compared to PTX**s** or BIBF**s** as single agents. These data substantiate the dependence of the combination of PTX and BIBF on LOF p53 status.

Emerging studies suggest that sequential or time-staggered drug administration, i.e., "molecular priming," may improve therapeutic efficacy[26]. However, concomitant administration of PTX**s** and BIBF**s** was superior to sequential administration (Fig. 1b). Thus, synthetic lethality does not require molecular priming with BIBF. Calculation of the combination index demonstrated pronounced synergy between PTX and BIBF at concentrations as low as 100 nM (Fig. 1c).

2 Preparation and characterization of PTX-loaded nanoparticles

Next, we designed a delivery system to enhance the cytotoxic effect of these drugs and overcome the drawbacks of administering soluble drugs in vivo. We chose polymeric NP due to their ability to offer superior drug stability, higher accumulation in the tumor, enhanced tumor regression, and lower systemic side effects as compared to soluble drug[27].

Biocompatible poly [lactic-co-glycolic acid] (PLGA) NP were prepared utilizing: 1) two different PLGA polymers of different monomer ratios and different molecular weights (Mw, (75:25, Mw= 67 kDa and 50:50, Mw= 24–38 kDa), and 2) two different surfactants: polyvinyl alcohol (PVA), and D-α-tocopherol polyethylene glycol 1000 succinate (TPGS). PVA is the most commonly used surfactant in NP fabrication based on its superior surfactant characteristics[28]. TPGS is a promising surfactant that has been recently used in NP fabrication, with a distinct ability to inhibit P-glycoprotein (P-gp) efflux transporter[29].

PTX-loaded NP were prepared using a nanoprecipitation method (Fig. 2a), a simple technique capable of producing small nanometer scale particles with narrow size distribution to more easily predict the in vivo behavior of the NP.

NP size <200nm potentiates passive targeting to the tumor via the EPR effect, which increases tumor cytotoxicity in vivo compared to soluble drugs[25]. All NP were <175 nm in diameter, with narrow size distribution and negative charge (Table 1). When TPGS was used as the surfactant, NP exhibited smaller hydrodynamic diameters relative to PVA. PTX loading into NP (PTX**p**) did not significantly alter size or zeta potential compared to blank NP (Blank**p**). PTX**p** prepared using PLGA (75:25) and TPGS (PTX**p** (75/T)) exhibited 1.8-times higher encapsulation efficiency (EE) and drug loading (DL) compared to PTX**p** prepared with PVA (PTX**p** (75/P)). The same trend was achieved when PLGA (50:50) was used to prepare NP, and thus a 1.6-fold higher EE and DL was achieved with TPGS (PTX**p** (50/T)) compared to PVA (PTX**p** (50/P)). The higher EE and DL with TPGS are likely due to the increased affinity of PTX for the hydrophobic vitamin E portion of TPGS embedded in the NP matrix[30]. Higher EE and DL were associated with the use of PLGA (75:25) when compared to PLGA (50:50) when the same surfactant was utilized, which is likely due to the higher lactic acid content and therefore superior hydrophobic characteristics.

All formulations were spherical with smooth surfaces, and loading PTX in the NP did not affect the integrity or surface morphology as compared to Blank**p** (Fig. 2b). There was no significant difference in size between TPGS- and PVA-prepared NP (e.g. Fig. 2b, panels 1&2). The discrepancy in NP size estimated using zeta sizer measurements (Table 1) versus SEM imaging is likely due to the fact that the hydrodynamic diameter, as measured by the zeta sizer, tends to overestimate the size of NP with hydrophilic surfaces. PVA has a higher hydrophilic lipophilic balance value of 18 as compared to 13.2 for TPGS[31], and thus the higher hydrophilic characteristics and higher hydrodynamic diameter values with PVA relative to TPGS were expected. Confocal imaging confirmed uptake of rhodamine B (RHD)-loaded NP (RHD**p**) by Hec50co cells (Fig. 2c, d). TEM images of PTX**p** (75/T) confirmed that the particles were spherical and <175 nm in size (Fig. 2e). In cells treated with PTX**p** (75/T), TEM images confirmed uptake (black arrows) and cytoplasmic distribution (Fig. 2f).

We next studied cytotoxicity as compared to PTX**s**. In Ishikawa and KLE cells, NP showed comparable decreases in cell viability relative to PTX**s**, with the exception of PTX**p** (50/T) which exhibited a 36% enhancement in cytotoxicity in KLE cells compared to PTX**s** (Fig. 3a). Interestingly, in Hec50co cells, all NP formulations except PTX**p** (50/P) promoted a significant decrease in cell viability, with the most notable effects being with TPGS-

emulsified NP (Fig. 3a). Dose response curves validated these findings (Fig. 3b). Studies using Blank**p** confirmed that the cytotoxicity was not due to the NP formulation (Fig. 3c). These data demonstrate that PTX**p** were specific for Hec50co cells with LOF p53 and were superior to PTX**s**.

Our data also demonstrate that TPGS is superior to PVA in LOF p53 cells. Since TPGS has been reported to inhibit drug efflux transporters[29], we hypothesized that the improved cell killing with PTX**p** (75/T) and PTX**p** (50/T) is due to increased intracellular retention of PTX. To test this, we performed flow cytometry cell uptake experiments utilizing RHD**p**. As with PTX[32], RHD is a substrate for the P-gp efflux transporter[33] and can serve as a surrogate for PTX intracellular behavior. In all three cell lines, RHD accumulation was increased with the use of TPGS as surfactant as compared to PVA (Fig. 3d). For example, the median fluorescence intensity of RHD**p** (75/T) in Hec50co cells was 11.4-times higher than that of RHD**p** (75/P), supporting our hypothesis that TPGS increases intracellular drug accumulation.

In addition, RHD**p** (75/T) exhibited 5.1-fold increase in fluorescence intensity when compared to RHD**p** (50/T), indicative of a difference in uptake. This could be related to the fact that PLGA (72:25) is more hydrophobic than PLGA (50:50)[34]. Indeed, both Ishikawa and KLE exhibited the same trend in NP uptake, though the magnitude of NP uptake was much higher in KLE cells (similar Hec50co). Based on these data, we surmise that Hec50co and KLE cells have higher expression of efflux transporter(s) relative to Ishikawa cells. Although KLE cells had higher accumulation of RHD**p** (75/T) (Fig. 3d), this was not reflected in higher cytotoxicity (Fig. 3a). This could be related to the fact that KLE cells are insensitive to PTX when compared to Hec50co cells (Fig. S2).

NP with a higher Mw PLGA (75:25) had a slower release profile for PTX compared to the lower Mw (50:50) polymer (Fig. 3e). These data are consistent with previous results that the higher the Mw of the polymer, the longer the polymer chain, the more hydrophobic the polymer, and subsequently the slower the degradation and the release of the loaded drug[35]. In addition, polymers with a higher lactic acid content, like PLGA (75:25), have a higher hydrophobicity and consequently slower interaction with water and slower degradation and drug release[35].

At the 24h time point, PTX release was slightly higher from PTX**p** (75/T) than PTX**p** (75/P). The apparent accelerated drug release with TPGS could be due to two possibilities. First, PTX has a high affinity for the vitamin E moiety of TPGS, which is expected to be oriented on the surface of the NP. This would increase the availability of PTX for release as compared to PVA-emulsified NP[30]. Another explanation is based on the reported faster release of docetaxel from TPGS-emulsified PLGA NP. TPGS forms pores at the NP surface and thus increases the exposed surface area to the release media[36].

In separate experiments using a well-established efflux transporter blood-brain barrier model, we confirmed that the RHD**p** (75/T) formulation has a robust uptake profile as compared to RHD**s** (Fig. S3). We also established that PTX**p** (75/T) significantly decreased cell viability in a cell model of paclitaxel resistance (Fig. S4). Marked cell death in cells

treated with PTX**p** (75/T) but not Blank**p** (75/T) was confirmed using multiple methods (Fig. S5).

3 PTXp induce synthetic lethality when combined with BIBF in LOF p53 USC

PTX**p** (75/T) was selected as the optimum formulation and used in subsequent combinatorial experiments with BIBF. We first explored the effect of combinatorial treatment on cell cycle progression in Hec50co cells. PTX**p** (75/T) promoted accumulation in G2/M, and addition of BIBF**s** resulted in nearly all cells accumulating at G2/M (Fig. 4a). In addition to effects on the G2/M checkpoint, BIBF has been reported to inhibit the P-gp efflux transporter[37], which would prevent PTX efflux and increase its intracellular concentration.

We next evaluated key G2/M regulators to determine if the combinatorial treatment abrogates the G2/M checkpoint. Phosphorylation of the kinase CDC2 at Tyr15 maintains the G2/M checkpoint, whereas dephosphorylation by the phosphatase CDC25C results in entry into M phase. CDC25C is maintained in an inhibited state through phosphorylation at Ser216, which is mediated by multiple kinases including p38MAPK. Abrogation of the G2/M checkpoint requires dephosphorylation of CDC25C at Ser216 and phosphorylation at 12 different sites (indicated by a slower migrating band) and dephosphorylation of CDC2 at Tyr15. Dual treatment with BIBF**s** and PTX**p** (75/T) resulted in decreased CDC2 Tyr15 phosphorylation and increased CDC25C activation (Fig. 4b). We also detected increased phosphorylation of the mitosis marker histone, H3.

Consistent with the data in Figure 1, dual treatment produced the most profound decrease in cell viability compared to either drug alone (Fig. 4c, left panel), indicative of synthetic lethality. In contrast to parental Hec50co cells, Hec50co cells expressing a GOF p53 mutant did not show any additional increase in cytotoxicity from the combinatorial treatment over PTX**p** (75/T) alone (Fig. 4c), demonstrating the requirement for LOF p53 status for synthetic lethality.

The difference in toxicities due to p53 status could be attributed to two possibilities. 1) In the absence of p53, cells rely on the p38 pathway to maintain the G2/M checkpoint[14,16], and treatment with a TKI in combination with PTX reduces p38 activation[16,38]. In the GOF p53 cells, cells have evolved an additional mechanism to maintain p38 activation through increased expression of the upstream kinase MKK3[16]. Hence, treatment with a TKI is not sufficient to abrogate the G2/M checkpoint. 2) The change in p53 status is accompanied by a change in the expression of efflux transporter(s) and thus corresponding differences in PTX intracellular accumulation. Given that BIBF inhibits P-gp[37], this change in drug efflux would alter the cytotoxicity of the combination therapy. The relationship between P-gp expression and p53 status is controversial: Thottassery et al showed that LOF p53 is associated with upregulation of P-gp[39], whereas Angelis et al showed that there is no correlation[40]. In addition, a positive correlation between GOF p53 and P-gp overexpression has been reported by Sampath and colleagues[41].

We therefore performed a cell uptake experiment to examine if BIBF**s** increases the drug accumulation using RHD**p** as a surrogate. BIBF**s** significantly enhanced the accumulation of RHD inside both parental and GOF Hec50co cells for all tested formulations (Fig. 4d&e), with a similar magnitude of increase in both cell lines. These data support the interpretation that the synthetic lethality observed in (Fig. 4c) is likely due to interference with the G2/M checkpoint in LOF p53 cells.

4 In vivo synthetic lethality and safety of PTXp+BIBFp

We generated PLGA (75/T) NP loaded with BIBF (denoted as "BIBF**p** (75/T)"). NP size, zeta potential and encapsulation efficiency are summarized in Table 1. SEM of the BIBF**p** (75/T) demonstrated spherical NP with a smooth surface morphology (Figure S6). The combination therapy of PTX**p** (75/T) + BIBF**p** (75/T) promoted a marked decrease in cell viability compared to all other treatments, including PTX**p** (75/T) + BIBF**s** (Fig. 5a). Thus, BIBF administered in NPs does not impact synthetic lethality to PTX**p** (75/T). Like PTX, BIBF is a reported substrate of P-gp[42], and loading BIBF in NP containing TPGS may increase its intracellular accumulation and therapeutic effect.

Studies were extended to an in vivo xenograft model of USC using Hec50co cells. PTX**p** (75/T) alone impeded tumor growth more than PTX**s**, indicating that delivery of PTX in a NP formulation improves efficacy (Fig. 5b). Treatment with PTX**p** (75/T) + BIBF**p** (75/T) was superior to PTX**p** (75/T) alone, supporting that the combination of BIBF and PTX induces synthetic lethality in vivo. Only the combination therapy of PTX**p** (75/T) + BIBF**p** (75/T) significantly inhibited tumor growth as compared to PTX**s** and naïve control. Representative images of mice at day 32 are shown in Fig. 5c.

The combination was the only treatment that significantly increased median survival compared to the naïve group (Fig. 5d). Specifically, treatment with PTX**p** (75/T) + BIBF**p** (75/T) was associated with a median survival of 51 days compared to 43, 41 and 39 days when mice were treated with PTX**p** (75/T), PTX**s** or saline, respectively. The 18.6% increase in median survival with the combination therapy versus PTX**p** (75/T) is in line with a clinical study of NSCLC demonstrating that the combination of BIBF and docetaxel extends survival by 22.3% compared to docetaxel plus placebo[22]. This effect was only observed in NSCLC patients with adenocarcinoma histology. Since *TP53* mutations also predominate in the adenocarcinoma subtype of NSCLC[43], we speculate that NSCLC patients that responded in this trial may harbor LOF p53, supporting that the concept of synthetic lethality may be applicable to cancers beyond USC.

The in vivo safety of the combination therapy is supported by stable body weight (Fig. 5e) and the absence of signs of necrosis or cell death in the heart, lung, liver, spleen or kidney as measured by H&E (Fig. 5f).

We also analyzed PTX intra-tumoral drug accumulation using a validated LC-MS/MS method (Fig. S7) and found superior accumulation of PTX**p** (75/T) compared to PTX**s** (Fig. 5g). Finally, we examined the biodistribution profile of NP loaded with a near infrared fluorescent dye (DIR) since previous studies have suggested that only a minor fraction of NP

(0.7%) reaches the tumor[44]. However, at least 10% of DIR**p** (75/T) accumulated in tumors (Fig. S8). Together, these data substantiate the potential clinical relevance of our preclinical studies.

5 Conclusions

The data presented here provide compelling evidence that p53 plays a critical role in response to the combination therapy of PTX and BIBF, such that synthetic lethality only occurs in the setting of LOF p53. Mechanistic studies support that abrogation of the G2/M checkpoint allows cells to prematurely enter M phase, where they undergo cell death through mitotic arrest. Moreover, the specific NP formulation consisting of PLGA at a monomer ratio of 75:25 and TPGS surfactant improves therapeutic efficacy through enhanced drug uptake and accumulation, and reduced drug efflux. Together, this conceptual design resulted in increased cell killing in vitro and decreased tumor growth in vivo without compromising safety.

A well-established mechanism of action for BIBF is its anti-angiogenic properties[21], which is relevant for the in vivo experiments. However, anti-angiogenic activity has been reported after administration of BIBF at a dose of 100 mg/kg orally for five consecutive days[21]. In our studies, we administered BIBF only once per week, which would likely not be sufficient for an anti-angiogenic effect.

Numerous EC clinical trials have explored the use of small molecule inhibitors as single agents. To date, only a handful of treatments have improved survival, with the best results seen with anti-angiogenic agents (bevacizumab[45], cediranib[46]). However, it should be noted that these treatments only extend progression free survival on average by three months. These data suggest that combinatorial strategies that target specific Achilles' heels in each tumor must be designed in order to improve long-term survival for patients with EC. Data from this study provide the proof-of-concept that synthetic lethality to PTX can be achieved in LOF p53 tumors by the addition of BIBF to the treatment regimen. These findings may extend beyond EC to other cancers types that are typified by *TP53* mutations, such as NSCLC and ovarian cancer, where the combination of BIBF with chemotherapy has improved survival[22,23].

11 Materials and methods

Cell culture

Ishikawa H (Ishikawa, type I EC) and Hec50co EC cells (USC), a subline of Hec50 cells, were kindly provided by Dr. Erlio Gurpide (New York University)[47,48], and KLE cells (USC) were purchased from American Type Culture Collection (ATCC, Manassas, VA). Hec50co cells stably expressing p53 R175H GOF (GOF Hec50co, USC) have been previously described[15]. Ishikawa and Hec50co cells were cultured in Dulbecco's modified Eagle's medium (Gibco, Invitrogen, Waltham, Ma) supplemented with 1% Pen/Strep (100 U/mL, Gibco) and 10% FBS (Atlanta Biologicals, Lawrenceville, GA). KLE cells were cultured in RPMI-1640 medium (Gibco) supplemented with 1% Pen/Strep and 10% FBS. GOF Hec50co cells were cultured as Hec50co cells with the addition of 0.8 mg/mL G418 to

main stable p53 R175H expression (Gibco). All cells were maintained in a humidified incubator (Sanyo Scientific Autoflow, IR direct heat CO_2 incubator) at 37 °C under 5% CO_2 flow. All cell lines were authenticated by CODIS marker testing, and were mycoplasma-free as determined by MycoAlert mycoplasma detection kit (Lonza, Rockland, ME).

Cell viability assay

Two days prior to adding the treatments, Ishikawa, Hec50co and GOF Hec50co cells were plated at a density of 10^3 cells/well, while the slower growing KLE cells were plated at 0.5×10^4 cells/well, in 96 well plates. Treatments were added in a volume of 50 μL/well followed by the addition of 150 μL/well of fresh media. Untreated control group was incubated with 200 μL/well of fresh media. Three days later, the contents of the 96 well plates were aspirated, replaced by 100 μL of fresh media and 20 μL of MTS reagent in each well (CellTiter 96 Aqueous One Solution Reagent, Promega Corporation, Madison, WI), and incubated at 37°C with 5% CO_2 for 1–4 h. The absorbance was recorded at 490 nm using a Spectra Max plus 384 Microplate Spectrophotometer (Molecular Devices, Sunnyvale, CA). Relative cell viability values were expressed as the percentage of the absorbance from the treated wells compared to the control wells (untreated), given that the control wells viability were set to 100%. For experiments where both concomitant and sequential administration of PTX and BIBF were evaluated (Fig. 1b), Hec50co cells were seeded at 10^3 cells/well for 48 h. The first treatment was added for another 48 h, washed away and then the second treatment was added for extra 72 h, followed by assessment of viability. The untreated control group was incubated with fresh media for 5 days. Synergy between PTX**s** and BIBF**s** was evaluated in Hec50co cells through the establishment of dose response curves of PTX**s**, BIBF**s** or the combination using varied concentrations of PTX**s** and either 1 μM BIBF**s** or 100 nM BIBF**s**. Cytotoxicity was estimated using MTS assay as stated above. Combination index (CI) values were calculated by utilizing the dose response curve data in CompuSyn software (ComboSyn, Inc., Paramus, NJ): a CI<1 indicates synergy.

NP fabrication and characterization

(a) NP fabrication—NP were prepared using nanoprecipitation method as diagrammed in (Fig. 2A). Briefly, 5 mg of drug (paclitaxel (PTX) (LC Laboratories, Woburn, MA) or BIBF 1120 (BIBF) (Selleck Chemicals, Houston, TX)) and 100 mg of polymer (poly [lactic-co-glycolic acid] (PLGA, 75:25, Mw, of 68 kDa, inherent viscosity of 0.59 dL/g, Durect Corporation, Pelham, Al)) or PLGA (50:50, Mw of 24–38 kDa, inherent viscosity of 0.32–0.44 dL/g, Resomer RG 503H, Boehringer Ingelheim KG, Germany)) were dissolved in 4.25 mL acetone (Fisher Scientific, Waltham, MA), and 0.75 mL of 97% ethanol (Sigma-Aldrich, St. Louis, MO, USA). This organic phase was added to a 10 mL syringe, with a needle size of G26, placed such that the tip was submerged just below the surface of stirred 50 mL of aqueous solution containing 0.1% w/v surfactant (Poly(vinyl alcohol) (PVA, Mw 8–9 kDa, 80% hydrolyzed, Sigma) or D-α-tocopherol polyethylene glycol 1000 succinate (TPGS, Sigma)) in a 150 mL beaker. The formed suspension was left on the stirrer for 45 min and then the rest of the organic solvent was evaporated under reduced pressure of 40 mbar using Laborota 4000 rotary evaporator (Heidolph, Schwabach, Germany) for 4 h. NP were then washed with nanopure water and collected using Amicon ultra-15 centrifugal filter units (Mw cutoff =100 kDa, EMD Millipore, Billerica, MA) at 500xg for 15 min 4 times using an

Eppendorf centrifuge 5804 R (Eppendorf, Westbury, NY). NP were freshly prepared before each experiment. For (Fig. 3 a&b) PTX**p** (75/T) and PTX**p** (75/P) were prepared on the first day, stored overnight at 4°C, and then PTX**p** (50/T) and PTX**p** (50/P) were prepared on the second day, when all the treatments were initiated. This staggered preparation was due to experimental limitations associated with NP fabrication, as preparation of each batch takes ~ 6–7 h.

(b) Estimation of drug loading and encapsulation efficiency—NP were dissolved in acetonitrile and drug content was estimated through HPLC-UV for PTX and HPLC-MS for BIBF. PTX content in the NP was quantified using HPLC-UV (2690 Alliance separation module coupled with 2487 dual λ absorbance detector, Waters, Milford, MA). Reverse phase 5 μm C-18 column, 100 A°, 4.5 × 250 mm (Waters) was utilized in the assay and isocratic elution with a mobile phase of acetonitrile (Fisher Scientific): water (60:40, v/v) at a flow rate of 1 mL/min was used. The detection wavelength was set at 227 nm and the injection volume was 100 μL. BIBF content was determined using HPLC-Mass (Shimadzu Model 2010A liquid chromatograph and mass spectrometer, Shimadzu, Columbia, MD) using a LC-10AD VP Solvent Delivery system. Synergi 4 μm Polar-RP column, 80 A°, 2 × 150 mm (Phenomenex Inc, Torrance, California) was used. Isocratic elution was utilized with a mobile phase composed of water + 0.1% formic acid (Fisher Scientific): acetonitrile + 0.1% formic acid (50:50, v/v), at a flow rate of 0.2 mL/min. Electrospray ionization was used, m/z ratio of 540.5 was utilized, and 25 μL was injected.

Drug loadings and encapsulation efficiencies were calculated from the following formulas.

$$\text{Drug loading } \left(\frac{\mu\text{g of drug}}{\text{mg of NP}}\right) = \frac{\text{Amount of PTX in NP } (\mu\text{g})}{\text{Total weight of NP (mg)}}$$

$$\text{Encapsulation efficiency } (\%) = \frac{\text{Amount of PTX in NP (mg)}}{\text{Initial amount of PTX (mg)}} \times 100$$

(c) NP size and zeta potential determination—NP suspension of 0.05 mg/mL was prepared in water. Size and zeta potential were then measured using a Zetasizer Nano ZS particle analyzer (Malvern Instrument Ltd., Westborough, MA).

(d) Microscopic evaluation of NP

Scanning electron microscopy: Surface morphology of prepared NP was examined using scanning electron microscopy (SEM). Briefly, NP suspension of 0.05 mg/ml was added onto a silicon wafer mounted on an aluminum SEM stubs. The suspension was allowed to air dry for 24 h. They were then coated with gold and palladium by an argon beam K550 sputter coater (Emitech Ltd., Kent, England). Images were captured using the Hitachi S-4800 scanning electron microscope (Hitachi High-Technologies, Ontario, Canada), operated at 3kV accelerating voltage.

Confocal laser scanning microscopy: Qualitative cell uptake studies of the prepared NP were carried out using confocal microscopy. Briefly, rhodamine B (RHD, Sigma) loaded PLGA NP (RHD**p**) were prepared by the nanoprecipitation method as described previously, except that the drug was substituted by an equivalent amount of RHD. The RHD content in RHD**p** was calculated by dissolving the NP in DMSO and then comparing RHD fluorescence to a constructed calibration curve (data not shown). RHD fluorescence was measured at λex 540 nm and λem 625 nm using a SpectraMax M5 multi-mode microplate reader (Molecular Devices, Sunnyvale, CA). Hec50co cells were plated at density of 10^4 cells in a clear, flat-bottom, 4-chambered glass slides with a lid (Lab-Tek, Nunc, Rochester, NY), and incubated for 48 h (37°C, 5% CO_2). RHD loaded PLGA NP (RHD**p**) containing 0.01 μg RHD were then added to each chamber, leaving untreated cells as a control, and incubated with the cells for 4 h (cells in Z stacked confocal image were incubated for 24 h with RHD**p** (75/T), Fig. 2d). Media was removed and cells were washed twice with Hank's balanced salt solution (Gibco). Cell membranes were stained by adding 0.5 mL of prewarmed cell mask deep red plasma membrane stain solution (Invitrogen) at 5 μg/mL in each chamber, incubated for 5 min at 37°C, washed and replaced by 0.5 ml of fresh media for another 5 min. Media was then aspirated, washed twice with phosphate buffer saline (PBS, Gibco). Then 0.5 mL of 4% paraformaldehyde (Hatfield, PA, USA) fixative solution was added and incubated for 10 min at 37°C. The specimen was mounted with Vectashield Hardset medium containing DAPI (Vector laboratories, Burlingame, Ca) for staining the nuclei. The cellular fluorescence was observed using confocal laser scanning microscopy (Carl Zeiss 710, Germany) equipped with Zen 2009 imaging software. The images were processed using Image J open access software, version 1.47 (National Institutes of Health, MD).

Transmission electron microscopy: The size and shape of PTX loaded NP (PTX**p**) prepared from PLGA (75:25) and TPGS surfactant (PTX**p** (75/T)) were also measured by JEOL JEM-1230 transmission electron microscope (TEM) equipped with a Gatan UltraScan 1000 2k × 2k CCD acquisition system ((JEOL USA, Inc., Peabody, MA). 10 μL of NP suspension (0.05 mg/mL) was added for 30 secs on a carbon coated, glow discharged 400-mesh TEM copper grid by Auto 306 (BOC Edwards, Crawley, United Kingdom) that was pre-coated with a Formvar 0.5% solution in ethylene dichloride film (Electron Microscopy Sciences, Hatfield, PA). Whatman filter paper was then used to remove any excess liquid and the grid was air dried. The TEM images were processed using Image J.

Cellular uptake of PTX**p** (75/T) was further confirmed through TEM. HEC50co cells were seeded at 10^6 cells in a 100 mm petri dish for 24 h. PTX**p** (75/T) at concentration equivalent to 5 nM PTX were then incubated with the cells for another 24 h. Cells were then fixed with 2.5% glutaraldehyde (Electron Microscopy Science, EMS, Hatfield, PA) in 0.1 M sodium cacodylate buffer (EMS), pH 7.4, for 30 min, rinsed twice with 0.1 M cacodylate buffer, pH 7.4, for 4 min each. 1% osmium tetroxide (EMS) was then added for 30 min to increase electron density and improve fixation efficiency. Fixed cells were then washed twice with distilled water and stained with 2.5% uranyl acetate (EMS) for 5 min. Dehydration of the sample was performed gradually using 25%, 50%, 75%, 95% ethanol, each for 4 min, and finally twice with 100% ethanol for 5 min each. Dehydrated samples were infiltrated with

ethanol: Epon (Ted Pella, Inc., Redding, CA) mixture (1:1) for 30 min, and then embedded in Epon at 70°C for 8 h. Thin nanometer sections of 60–80nm were cut using Leica EM UC6 Ultramicrotome MZ6 (Reichert-Jung, Reichert, Depew, NY), finally these sections were mounted on Formvar-coated 400-mesh TEM copper grid, counter stained with 5% uranyl acetate and Reynold's lead citrate (80 mM lead nitrate (Sigma) in 164 mM sodium citrate buffer (RPI, Mt. Prospect, IL)). Sample was then imaged, and then processed using Image J.

(e) Quantitative uptake of NP by flow cytometry—Quantitative cell uptake was carried out using FACScan flow cytometer (Becton Dickinson, Franklin Lakes, NJ) and analyzed using FlowJo software (TreeStar, Inc., Ashland, OR). Ishikawa. Hec50co and GOF Hec50co cells were plated at density of 10^5 cells, while KLE cells were plated at density of 0.5×10^6 cells in 12 well plates. One day later, equivalent amount of RHD**p** containing 0.01 μg RHD was added to each well in serum free media, and untreated cells were used as control. 6 h later, cells were washed with PBS twice, trypsinized, quenched with serum containing media, centrifuged at 230 ×g for 5 min, resuspended in 300 μL of fresh media and kept on ice until analysis was performed. Serum free media was used to accelerate the uptake process of these particles and thus differences in the magnitude of NP uptake would be easily detected over a short period of incubation[49].

(f) PTX in vitro release—PTX release studies from different formulations were performed by adding PTX**p** equivalent to 1 μg PTX in 1 mL of 1% v/v aqueous tween 80 solution (Fisher Scientific) in 1.5 mL amber microcentrifuge tube. Samples were incubated at 37°C in a horizontal shaker at 300 rpm. At each time point, 3 tubes were centrifuged at 20817 ×g for 20 min at 5°C, the supernatant was discarded, and the amount of drug remaining in particles was estimated by dissolving the pellet in acetonitrile, vortexed for 10 min, and finally analyzed using HPLC. The total amount released at each time point was calculated by subtracting the amount of PTX remaining in the pellet from the original amount of PTX added to each tube.

Cell cycle analysis by flow cytometry

Cells were plated in 100 mm dishes with an equal number of cells in each dish and treated with either 1 μM of soluble BIBF (BIBF**s**), 40 nM of PTX**p** (75/T), or combination of both for 24 h. Cells were fixed in 70% ethanol. After washing with PBS, cells were incubated in Krishan's solution (3.8 mM sodium citrate (Fisher Scientific), 0.014 mM propidium iodide (AnaSpec, Fermont, Ca), 1% NP-40 (Sigma) and 2.0 mg/mL RNase A (Fisher Scientific) for 30minutes at 37°C and analyzed by FACScan flow cytometer as previously described[16]. The data were subjected to further analysis by CellQuest software version 3.3, which was used to generate DNA histograms indicating the fractions of the cell population in the sub-G1, G0-G1, S or G2/M phase of the cell cycle.

Western blot analysis

As previously described[16], cells were plated in 100 mm dishes and were allowed to grow for 24 h prior to adding the treatment. Cells were treated with either 1 μM of BIBF**s**, 40 nM of PTX**p** (75/T), or combination of both for 24 h, and then cells were harvested, lysed with

extraction buffer (1% Triton X-100 (Sigma), 10 mM Tris-HCl (Sigma) pH 7.4, 5 mM EDTA (Sigma), 50 mM NaCl (Sigma), 50 mM NaF (Fisher Scientific), 20 μg/ml aprotinin (Fisher Scientific), 1 mM PMSF (Fisher Scientific), and 2 mM Na3VO4 (Fisher Scientific)), and subjected to three freeze/thaw cycles. Equal amounts of protein (determined by the method of Bradford, BioRad, Hercules, CA) were subjected to SDS-PAGE (BioRad) followed by transfer to nitrocellulose membranes (BioScience, San Jose, CA). Membranes were probed with primary antibodies against total CDC2 (catalogue no. 9112), phospho-cdc2 Tyr 15 (catalogue no. 9111), CDC25C (catalogue no. 4688) and phospho-histone H3 Ser10 (catalogue no. 3377, Cell Signaling Technology, Danvers, Ma) followed by incubation with corresponding horseradish peroxidase-conjugated secondary antibody (catalogue no. 7074, Cell Signaling Technology). The signal was visualized by chemiluminescence using ECL Western blotting detection reagents (Pierce, Fisher Scientific).

BIBFs effect on NP uptake using flow cytometry

The effect of BIBF**s** on the uptake of different RHD**p** against Hec50co cells and GOF Hec50co cells was tested. Both cell lines were plated at a seeding density of 10^5 cell/ well in 12 well plate, and then the uptake experiment was carried out as stated previously with two exceptions: a) RHD**p** uptake was evaluated in the presence or absence of 1 μM BIBF**s**, b) the experiment was carried out in serum containing media to mimic the in vivo conditions.

In vivo efficacy studies using mouse xenograft model of LOF p53 USC

Female athymic NCI-nu/nu mice (Charles River, Wilmington, MA) at the age of 6–8 weeks were challenged subcutaneously with 2×10^6 Hec50co cells in the right flank after isoflurane anesthesia. Once the tumor volumes reached 50 mm^3, mice were randomized into four groups, and were then treated with either saline (naïve), 5 mg/kg PTX**s** in 10% (v/v) Tween 80 solution, 5 mg/kg PTX**p** (75/T), or the combination therapy of 5 mg/kg PTX**p** (75/T) and 5 mg/kg BIBF**p** (75/T). Mice were 5 per group, except the group that received the combination therapy were 7. Treatments were administered IV through retro-orbital injections in the venous sinus on days 18, 25, and 32. The tumor diameters and height were measured using digital caliper. The tumor volumes were calculated from the following formula:

$$\text{Tumor volume } (\text{mm}^3) = \frac{\pi}{6} \times \text{D}_1 \times \text{D}_2 \times \text{H}$$

Where D_1 and D_2 are first and second tumor diameters (mm), respectively, and H is the tumor height (mm).

Mice weights were monitored during the experiment and mice were euthanized once the tumor diameter exceeded 2 cm or tumor height exceeded 1 cm. Sample sizes for this experiment were estimated based on preliminary data in order to have 80% power to detect significant differences between groups. All animal experiments were not blinded, and were carried out in accordance with guidelines and regulations approved by the University of Iowa Institutional Animal Care and Use Committee.

Histological evaluation of the NP safety

Once tumor-challenged mice were euthanized, heart, lung, liver, spleen and kidney were harvested, fixed in 10% neutral buffered formalin (RPI), and then embedded in paraffin (EM-400, Surgipath, Leica Biosystems, Inc., Buffalo Grove, IL). Sections of 5 μm were prepared, stained with H&E (Leica), and imaged using Olympus BX61 microscope (Olympus, Center Valley, PA). Finally, images were processed using Cell Sens software (Olympus).

Estimation of PTX intra-tumoral drug concentration

Female athymic NCI-nu/nu mice at the age of 6–8 weeks were challenged subcutaneously with 2×10^6 Hec50co cells in the right flank after isoflurane anesthesia. Once the tumor volumes reached ~500 mm^3, mice were IV (retro-orbital injection) treated with either 5 mg/kg PTX**s** or 5 mg/kg PTX**p** (75/T). Tumors were collected 1, 4 and 12 h post injection, and PTX concentration within the tumor was quantified using a validated LC-MS/MS method (Fig. S8).

Statistical analysis

All in vitro experiments were repeated twice (n=3 biological replicates). Data are expressed as mean ± SEM. Statistical analysis was performed using GraphPad prism software for Windows version 6.07 (GraphPad Software, Inc., San Diego, CA). Unpaired two-tailed t-test was used to compare between two groups, and one-way analysis of variance (ANOVA) followed by Tukey post hoc test was used to compare between 3 or more groups. In vivo tumor progression curves were analyzed utilizing the non-parametric Kruskal-Wallis test. Kaplan-Meier survival curves were analyzed using the Log-rank test with the Bonferroni post hoc test. Differences were considered significant at $p < 0.05$.

Data availability

All the data generated or analyzed during this study are included in this published article (and its supplementary information files).

Supplementary Material

Refer to Web version on PubMed Central for supplementary material.

Acknowledgments

This work was supported by the National Cancer Institute at the National Institutes of Health (P50 CA97274/ UI Mayo Clinic Lymphoma SPORE grant to A.K.S., P30 CA086862 Cancer Center support grant to A.K.S., R01 CA099908 to K.K.L. and R01 CA184101 to X.M. and K.K.L.), the Lyle and Sharon Bighley Professorship (A.K.S.) and the Department of Obstetrics and Gynecology Research Fund (K.K.L.). K.E. acknowledges the Egyptian Ministry of Higher Education for a graduate fellowship award. We would like to acknowledge the University of Iowa Central Microscopy Research Facility staff and especially Katherine Walters for her help with histological analysis data. The flow cytometry data were obtained at the Flow Cytometry Facility, which is a Carver College of Medicine/Holden Comprehensive Cancer Center core research facility at the University of Iowa.

References

1. Cancer facts and figures 2017. 2017. https://www.cancer.org/content/dam/cancer-org/research/cancer-facts-and-statistics/annual-cancer-facts-and-figures/2017/cancer-facts-and-figures-2017.pdf
2. Doll A, et al. Novel molecular profiles of endometrial cancer-new light through old windows. J. Steroid Biochem. Mol. Biol. 2008; 108:221–229. [PubMed: 18061438]
3. Hamilton CA, et al. Uterine papillary serous and clear cell carcinomas predict for poorer survival compared to grade 3 endometrioid corpus cancers. Br. J. Cancer. 2006; 94:642–646. [PubMed: 16495918]
4. Boruta DM 2nd, Gehrig PA, Fader AN, Olawaiye AB. Management of women with uterine papillary serous cancer: a Society of Gynecologic Oncology (SGO) review. Gynecol. Oncol. 2009; 115:142–153. [PubMed: 19592079]
5. Dizon DS, et al. A phase II evaluation of nintedanib (BIBF-1120) in the treatment of recurrent or persistent endometrial cancer: An NRG Oncology/Gynecologic Oncology Group Study. Gynecol. Oncol. 2014; 135:441–445. [PubMed: 25312396]
6. Integrated genomic characterization of endometrial carcinoma. Nature. 2013; 497:67–73. [PubMed: 23636398]
7. Brachova P, Thiel KW, Leslie KK. The consequence of oncomorphic TP53 mutations in ovarian cancer. Int. J. Mol. Sci. 2013; 14:19257–19275. [PubMed: 24065105]
8. Agarwal ML, Agarwal A, Taylor WR, Stark GR. p53 controls both the G2/M and the G1 cell cycle checkpoints and mediates reversible growth arrest in human fibroblasts. Proc. Natl. Acad. Sci. U S A. 1995; 92:8493–8497. [PubMed: 7667317]
9. Jordan MA, Wilson L. Microtubules as a target for anticancer drugs. Nat. Rev. Cancer. 2004; 4:253–265. [PubMed: 15057285]
10. Kastan MB, Bartek J. Cell-cycle checkpoints and cancer. Nature. 2004; 432:316–323. [PubMed: 15549093]
11. Jackson SP, Bartek J. The DNA-damage response in human biology and disease. Nature. 2009; 461:1071–1078. [PubMed: 19847258]
12. Manke IA, et al. MAPKAP kinase-2 is a cell cycle checkpoint kinase that regulates the G2/M transition and S phase progression in response to UV irradiation. Mol. Cell. 2005; 17:37–48. [PubMed: 15629715]
13. Boutros R, Lobjois V, Ducommun B. CDC25 phosphatases in cancer cells: key players? Good targets? Nat. Rev. Cancer. 2007; 7:495–507. [PubMed: 17568790]
14. Reinhardt HC, Aslanian AS, Lees JA, Yaffe MB. p53-Deficient Cells Rely on ATM- and ATR-Mediated Checkpoint Signaling through the p38MAPK/MK2 Pathway for Survival after DNA Damage. Cancer Cell. 2007; 11:175–189. [PubMed: 17292828]
15. Meng X, et al. Strategies for Molecularly Enhanced Chemotherapy to Achieve Synthetic Lethality in Endometrial Tumors with Mutant p53. Obstet. Gynecol. Int. 2013; 2013:828165. [PubMed: 24381593]
16. Meng X, et al. Induction of mitotic cell death by overriding G2/M checkpoint in endometrial cancer cells with non-functional p53. Gynecol. Oncol. 2013; 128:461–469. [PubMed: 23146687]
17. Kaelin WG. The Concept of Synthetic Lethality in the Context of Anticancer Therapy. Nat. Rev. Cancer. 2005; 5:689–698. [PubMed: 16110319]
18. Tutt A, et al. Oral poly(ADP-ribose) polymerase inhibitor olaparib in patients with BRCA1 or BRCA2 mutations and advanced breast cancer: a proof-of-concept trial. Lancet. 2010; 376:235–244. [PubMed: 20609467]
19. McLornan DP, List A, Mufti GJ. Applying synthetic lethality for the selective targeting of cancer. N. Engl. J. Med. 2014; 371:1725–1735. [PubMed: 25354106]
20. Khoo KH, Verma CS, Lane DP. Drugging the p53 pathway: understanding the route to clinical efficacy. Nat. Rev. Drug Discov. 2014; 13:217–236. [PubMed: 24577402]
21. Hilberg F, et al. BIBF 1120: Triple Angiokinase Inhibitor with Sustained Receptor Blockade and Good Antitumor Efficacy. Cancer Res. 2008; 68:4774. [PubMed: 18559524]

22. Reck M, et al. Docetaxel plus nintedanib versus docetaxel plus placebo in patients with previously treated non-small-cell lung cancer (LUME-Lung 1): a phase 3, double-blind, randomised controlled trial. Lancet Oncol. 2014; 15:143–155. [PubMed: 24411639]
23. du Bois A, et al. Standard first-line chemotherapy with or without nintedanib for advanced ovarian cancer (AGO-OVAR 12): a randomised, double-blind, placebo-controlled phase 3 trial. Lancet Oncol. 2016; 17:78–89. [PubMed: 26590673]
24. Jain RK, Stylianopoulos T. Delivering nanomedicine to solid tumors. Nat. Rev. Clin. Oncol. 2010; 7:653–664. [PubMed: 20838415]
25. Acharya S, Sahoo SK. PLGA nanoparticles containing various anticancer agents and tumour delivery by EPR effect. Adv. Drug Deliv. Rev. 2011; 63:170–183. [PubMed: 20965219]
26. Lee MJ, et al. Sequential application of anticancer drugs enhances cell death by rewiring apoptotic signaling networks. Cell. 2012; 149:780–794. [PubMed: 22579283]
27. Wang G, et al. Controlled preparation and antitumor efficacy of vitamin E TPGS-functionalized PLGA nanoparticles for delivery of paclitaxel. Int. J. Pharm. 2013; 446:24–33. [PubMed: 23402977]
28. Mu L, Feng SS. A novel controlled release formulation for the anticancer drug paclitaxel (Taxol): PLGA nanoparticles containing vitamin E TPGS. J. Control. Release. 2003; 86:33–48. [PubMed: 12490371]
29. Duhem N, Danhier F, Preat V. Vitamin E-based nanomedicines for anti-cancer drug delivery. J. Control. Release. 2014; 182:33–44. [PubMed: 24631865]
30. Mu LS, P H, Ang SN, Feng SS. Study on surfactant coating of polymeric nanoparticles for controlled delivery of anticancer drug. Colloid Polym. Sci. 2004; 283:58–65.
31. Turk CT, Oz UC, Serim TM, Hascicek C. Formulation and optimization of nonionic surfactants emulsified nimesulide-loaded PLGA-based nanoparticles by design of experiments. AAPS PharmSciTech. 2014; 15:161–176. [PubMed: 24222270]
32. Szakacs G, Paterson JK, Ludwig JA, Booth-Genthe C, Gottesman MM. Targeting multidrug resistance in cancer. Nat. Rev. Drug. Discov. 2006; 5:219–234. [PubMed: 16518375]
33. Eytan GD, Regev R, Oren G, Hurwitz CD, Assaraf YG. Efficiency of P-glycoprotein-mediated exclusion of rhodamine dyes from multidrug-resistant cells is determined by their passive transmembrane movement rate. Eur. J. Biochem. 1997; 248:104–112. [PubMed: 9310367]
34. Samadi Moghaddam M, Heiny M, Shastri VP. Enhanced cellular uptake of nanoparticles by increasing the hydrophobicity of poly(lactic acid) through copolymerization with cell-membrane-lipid components. Chem. Commun. (Camb). 2015; 51:14605–14608. [PubMed: 26287526]
35. Dinarvand R, Sepehri N, Manoochehri S, Rouhani H, Atyabi F. Polylactide-co-glycolide nanoparticles for controlled delivery of anticancer agents. Int. J. Nanomedicine. 2011; 6:877–895. [PubMed: 21720501]
36. Zhu H, et al. Co-delivery of chemotherapeutic drugs with vitamin E TPGS by porous PLGA nanoparticles for enhanced chemotherapy against multi-drug resistance. Biomaterials. 2014; 35:2391–2400. [PubMed: 24360574]
37. Xiang QF, et al. Effect of BIBF 1120 on reversal of ABCB1-mediated multidrug resistance. Cell Oncol. (Dordr). 2011; 34:33–44. [PubMed: 21290212]
38. Rangarajan S, et al. Novel Mechanisms for the Antifibrotic Action of Nintedanib. Am. J. Respir. Cell Mol. Biol. 2016; 54:51–59. [PubMed: 26072676]
39. Thottassery JV, Zambetti GP, Arimori K, Schuetz EG, Schuetz JD. p53-dependent regulation of MDR1 gene expression causes selective resistance to chemotherapeutic agents. Proc. Natl. Acad. Sci. U S A. 1997; 94:11037–11042. [PubMed: 9380755]
40. De Angelis P, et al. P-glycoprotein is not expressed in a majority of colorectal carcinomas and is not regulated by mutant p53 in vivo. Br. J. Cancer. 1995; 72:307–311. [PubMed: 7640210]
41. Sampath J, et al. Mutant p53 cooperates with ETS and selectively up-regulates human MDR1 not MRP1. J. Biol. Chem. 2001; 276:39359–39367. [PubMed: 11483599]
42. Nintedanib. Aust. Prescr. 2016; 39:62–63. [PubMed: 27340326]
43. The Cancer Genome Atlas Research, N. Comprehensive molecular profiling of lung adenocarcinoma. Nature. 2014; 511:543–550. [PubMed: 25079552]

44. Wilhelm S, et al. Analysis of nanoparticle delivery to tumours. Nat. Rev. Mater. 2016; 1:16014.
45. Aghajanian C, et al. Phase II Trial of Bevacizumab in Recurrent or Persistent Endometrial Cancer: A Gynecologic Oncology Group Study. J. Clin. Oncol. 2011; 29:2259–2265. [PubMed: 21537039]
46. Bender D, et al. A phase II evaluation of cediranib in the treatment of recurrent or persistent endometrial cancer: An NRG Oncology/Gynecologic Oncology Group study. Gynecol. Oncol. 2015; 138:507–512. [PubMed: 26186911]
47. Albitar L, Pickett G, Morgan M, Davies S, Leslie KK. Models representing type I and type II human endometrial cancers: Ishikawa H and Hec50co cells. Gynecol. Oncol. 2007; 106:52–64. [PubMed: 17490735]
48. Nishida M. The Ishikawa cells from birth to the present. Hum. Cell. 2002; 15:104–117. [PubMed: 12703541]
49. Guarnieri D, Guaccio A, Fusco S, Netti PA. Effect of serum proteins on polystyrene nanoparticle uptake and intracellular trafficking in endothelial cells. J. Nanopart. Res. 2011; 13:4295–4309.

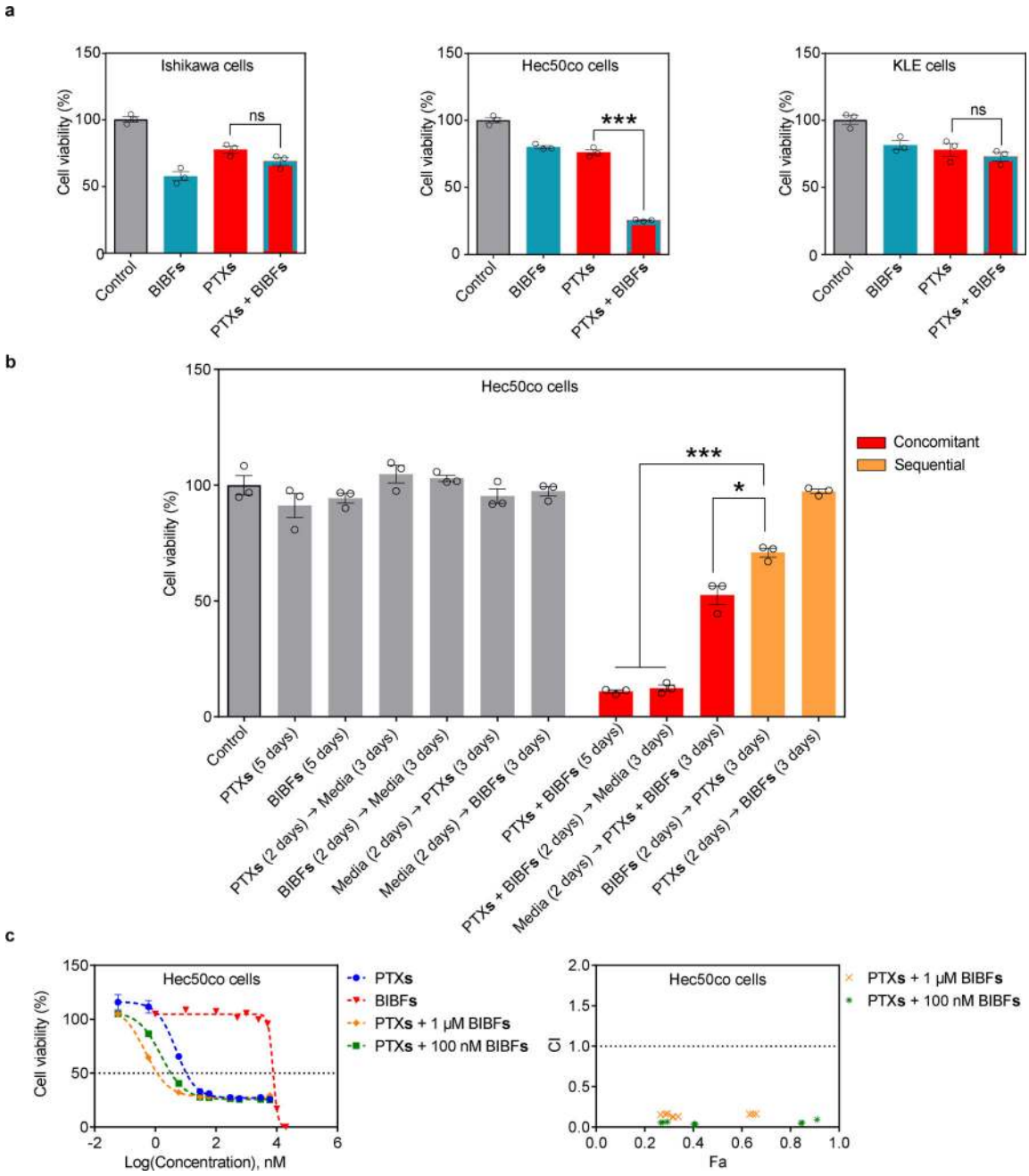

Figure 1.

Concomitant treatment of PTX**s** + BIBF**s** significantly inhibited cell growth only in EC cells with LOF p53 mutations. **(a)** Three EC cell lines were treated with PTX**s** and/or BIBF**s** for 72 h: Ishikawa cells; 5 nM PTX**s** and 2.5 μM BIBF**s**, Hec50co cells; 5 nM PTX**s** and 2.5 μM BIBF**s**, and KLE cells; 10 nM PTX**s** and 2.5 μM BIBF**s**. All combinatorial treatments were concomitant. **(b)** Sequential and concomitant treatments were also evaluated using Hec50co cells. PTX**s** and BIBF**s** doses were the same as in (a). The first treatment was added for 48 h, washed away, and then the second treatment was added for an additional 72 h. The untreated control group was incubated with fresh media for 5 days. **(c)** Synergy between PTX**s** and

BIBF**s** was evaluated in Hec50co cells. Left panel represents dose response curves of PTX**s**, BIBF**s** or the combination using varied concentrations of PTX**s** with either 1 μM BIBF**s** or 100 nM BIBF**s** for 72 h. Right panel represents combination index (CI) vs. fraction affected (Fa) curve; CI<1 indicates synergy. Cytotoxicity was determined using the MTS assay. Statistical analysis for panels A and B was performed using one-way ANOVA with Tukey post hoc test. Data are expressed as mean ± SEM (n=3). *** $p<0.001$, * $p<0.05$.

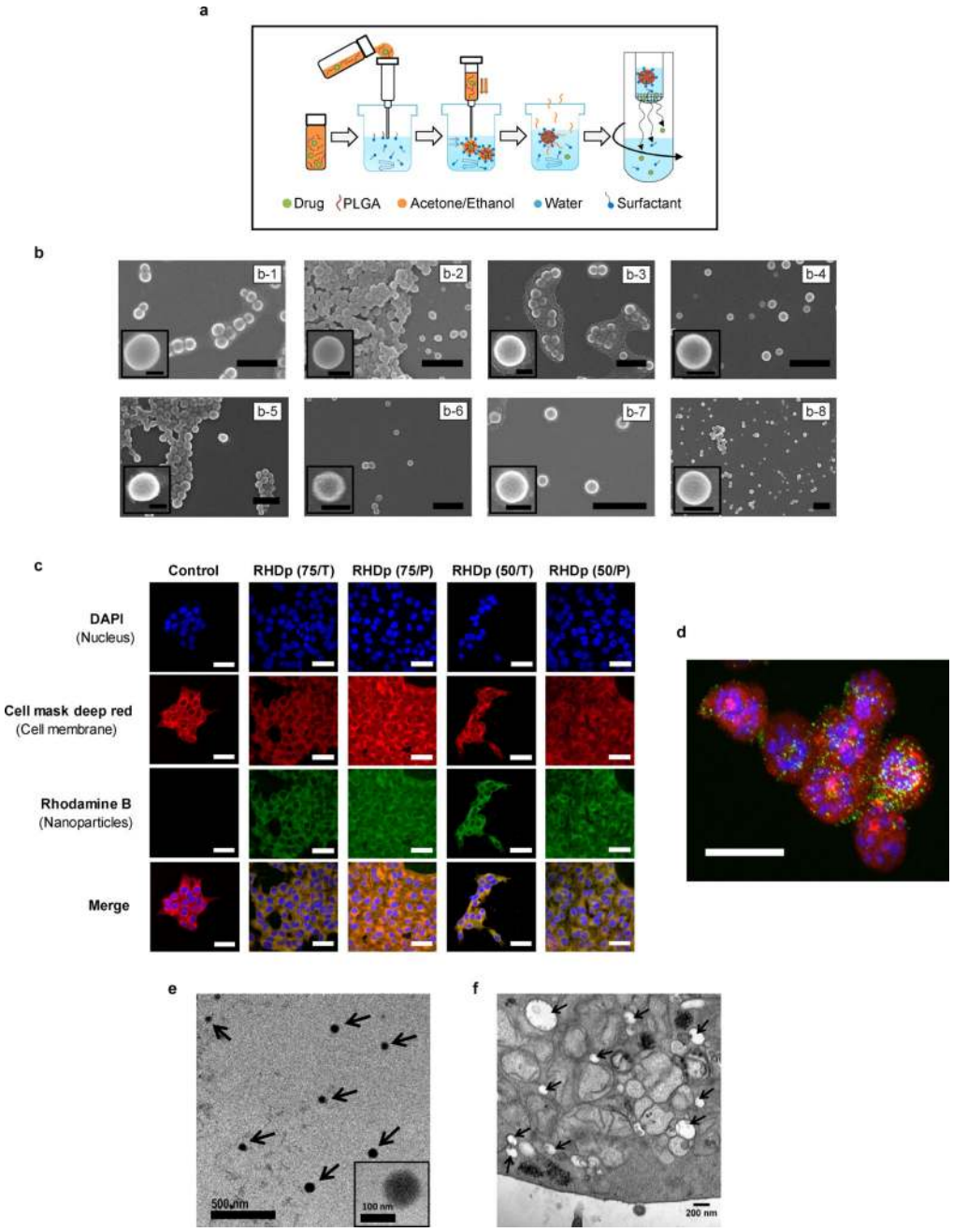

Figure 2.

PTX**p** were successfully prepared and microscopically characterized. **(a)** Schematic illustrating the nanoprecipitation method used for nanoparticle preparation. **(b)** Scanning electron micrographs of PTX**p** [b-1 to b-4] and Blank**p** [b-5 to b-8] showing spherically shaped nanoparticles with smooth surfaces. Scale bar = 500 nm [100 nm in the insert]. (b-1) PTX**p** (75/T), (b-2) PTX**p** (75/P), (b-3) PTX**p** (50/T), (b-4) PTX**p** (50/P), (b-5) Blank**p** (75/T), (b-6) Blank**p** (75/P), (b-7) Blank**p** (50/T), (b-8) Blank**p** (50/P). **(c)** Confocal microscopy images of Hec50co cells incubated with 4 different RHD**p** for 4 h. Blue: nucleus (DAPI), red: plasma membrane (cell mask deep red), green: RHD**p**. Scale bar = 50 μm. **(d)**

Z-stacked confocal image of Hec50co cells incubated with RHD**p** (75/T) for 24 h, utilizing same dyes as in (c). Scale bar = 25 μm. **(e)** Transmission electron micrographs of PTX**p** (75/T) showing spherical nanoparticles. Scale bar = 500 nm [100 nm in the insert]. **(f)** Transmission electron micrographs of Hec50co cells showing the uptake of PTX**p** (75/T) (black arrows) following 24 h incubation, validating that the confocal microscopy images were detecting NP and not simply free RHD that had leached out of the NP. Scale bar = 200 nm.

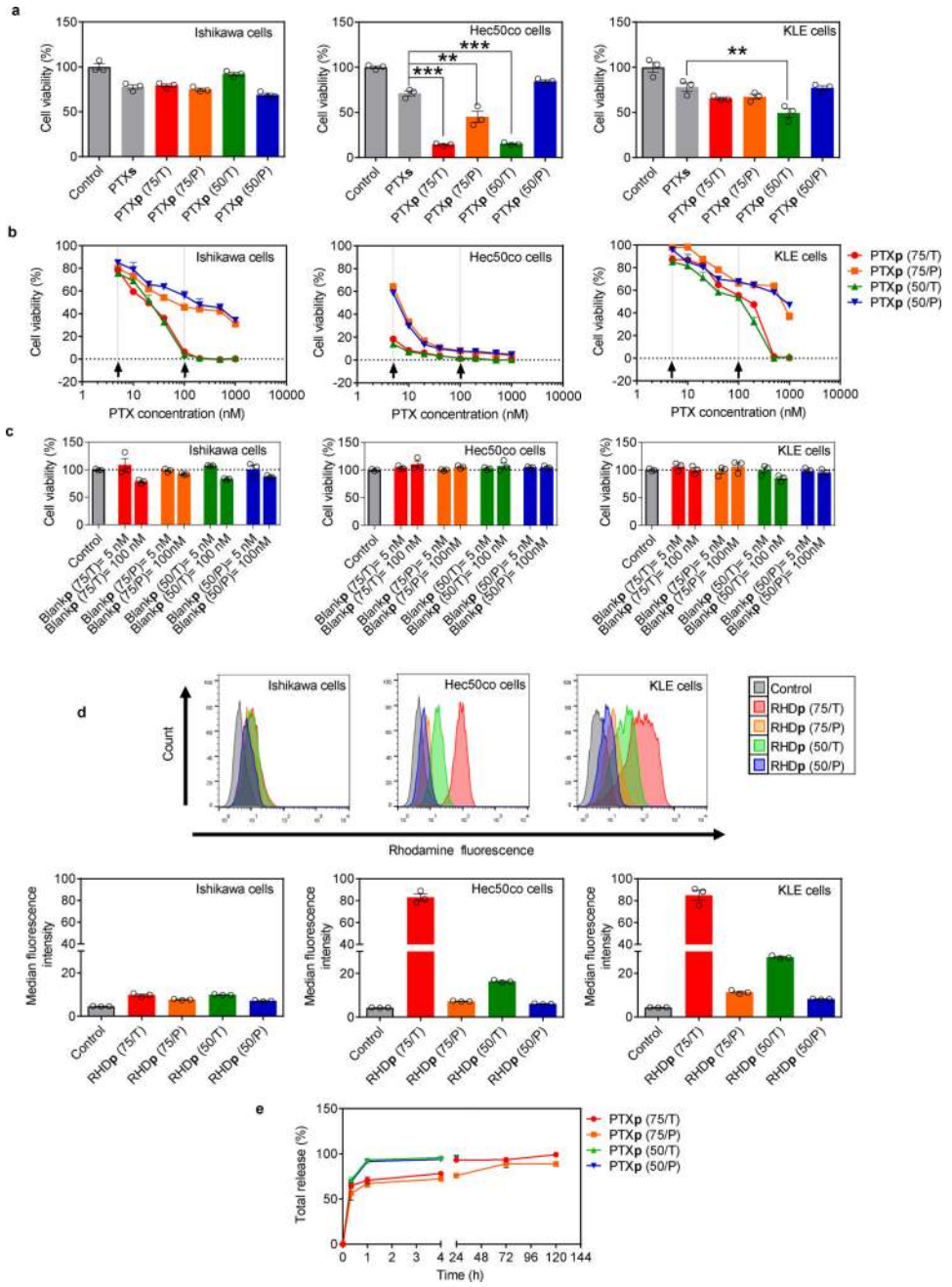

Figure 3.

PTX**p** (75/T) exhibited highest cell killing and uptake against Hec50co cells, in addition to slower drug release. **(a)** Cytotoxicity associated with the use of different PTX**p** formulations against three EC cell lines after 72 h of incubation. PTX dose: 5 nM in both Ishikawa and Hec50co cells, and 10 nM in KLE cells. Doses were selected based on the sensitivity of each cell line to PTX, in a way that ~75% cell viability is achieved with PTX**s** (see Fig. S2). **(b)** Dose response curve of different PTX**p** formulations against the three EC cell lines after 72 h of incubation. In both experiments (a) and (b), PTX**p** (75/T) and PTX**p** (75/P) were prepared on the first day, stored overnight at 4°C, and then PTX**p** (50/T) and PTX**p** (50/P)

were prepared on the second day, when all the treatments were initiated. **(c)** Cytotoxicity associated with the use of different Blank**p** formulations against three EC cell lines after 72 h of incubation. Doses of the Blank**p** were equivalent to 5 nM and 100 nM in the PTX**p** formulation. **(d)** Flow cytometry analysis for uptake studies of different RHD**p** formulations against three EC cell lines after 6 h of incubation in serum free media to maximize uptake of the NP and thus facilitate detection of any small difference between uptake of different NP formulations. Upper panels show histograms of different treatments. Lower panels show median fluorescence intensity of these histograms. **(e)** Release studies of different PTX**p** formulations in 1% v/v Tween 80 solution in phosphate buffered saline. Cytotoxicity in (a), (b) and (c) was determined using the MTS assay. Statistical analysis was performed using one-way ANOVA with Tukey post hoc test. Data are expressed as mean ± SEM (n=3). *** $p<0.001$, ** $p<0.01$.

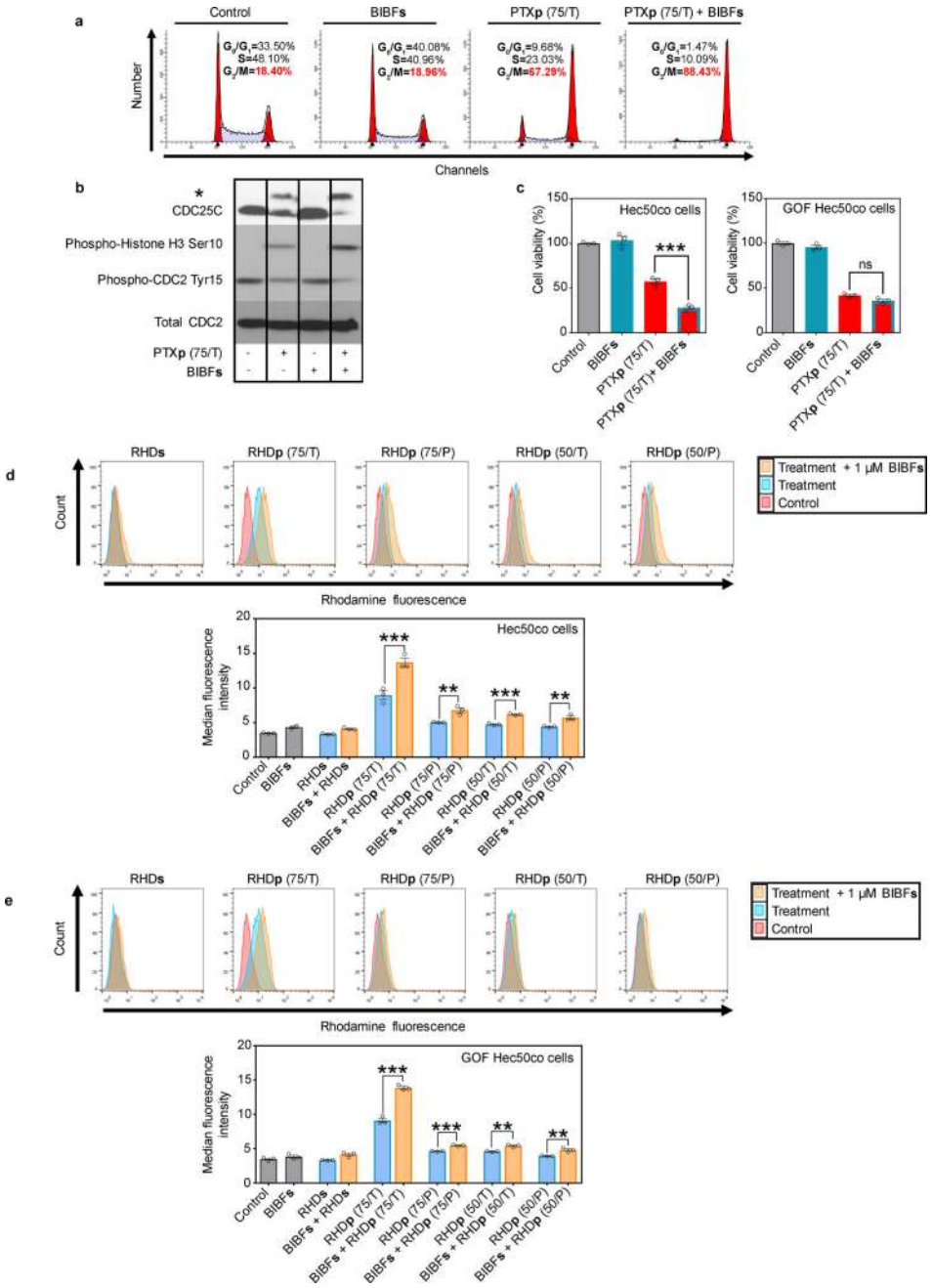

Figure 4.

BIBF**s** induced synthetic lethality to PTX**p** (75/T) in LOF p53 cells through the abrogation of the G2/M checkpoint. **(a)** Cell cycle profiles of Hec50co cells treated with either 1 μM BIBF**s**, 40 nM PTX**p** (75/T), or the combination of both for 24 h. The percentage of cells in G2/M transition is indicated in red in each plot. **(b)** Western blot analysis showing the effect of either 1 μM BIBF**s**, 40 nM PTX**p** (75/T), or the combination of both on the post translational modification of cell cycle regulators in Hec50co cells following 24 h incubation. * represents a slow migrating band of phosphorylated CDC25C. **(c)** Cytotoxicity associated with the use of 1 μM BIBF**s**, 5 nM of PTX**p** (75/T), or the combination of both

against Hec50co cells and GOF Hec50co cells, following 72 h incubation. Cytotoxicity was assessed using MTS assay. Statistical analysis was performed using one-way ANOVA with Tukey post hoc test. Data are expressed as mean ± SEM (n=3). *** $p<0.001$. **(d)** and **(e)** The effect of 1 μM BIBF**s** on the uptake of different RHD**p** formulations after 6 h incubation with **(d)** Hec50co cells, or **(e)** GOF Hec50co cells, as determined by flow cytometry. Complete media was used in this experiment to mimic in vivo conditions. Upper panels show histograms of different treatments, while lower panel shows median fluorescence intensity data of these histograms. Statistical analysis was performed using unpaired two-tailed t-test. Data are expressed as mean ± SEM (n = 3). *** $p<0.001$, ** $p<0.01$.

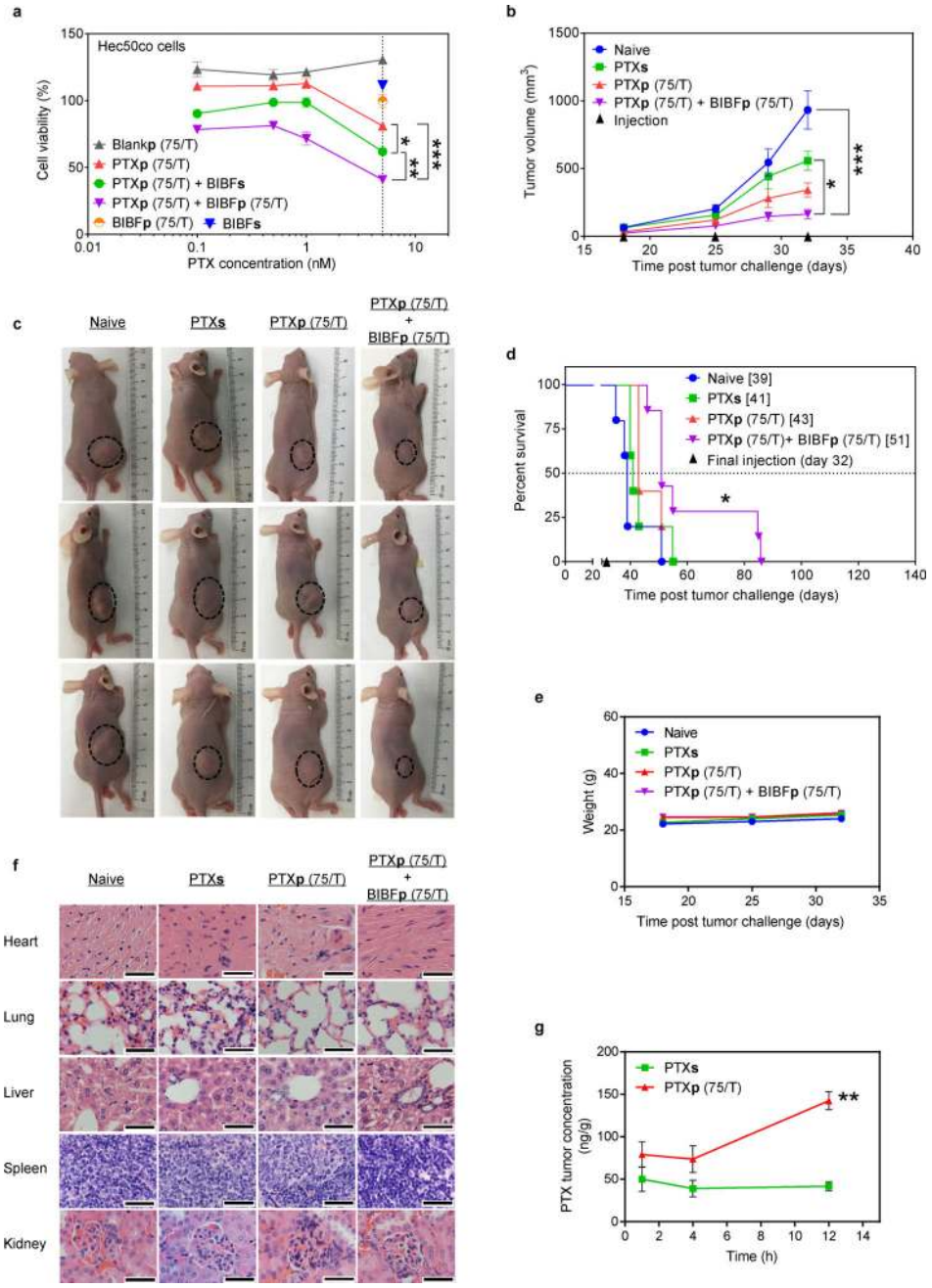

Figure 5.

The combination of PTX**p** (75/T) + BIBF**p** (75/T) demonstrated highest reduction in tumor progression, extended median survival and favorable safety in vivo. **(a)** Cytotoxicity associated with the use of 100 nM BIBF**s** or 100 nM BIBF**p** (75/T) in combination with different PTX concentrations against Hec50co cells, as measured by MTS assays. Indicated treatments involved incubation with cells for 72 h. Statistical analysis was performed using one-way ANOVA with Tukey post hoc test. Data are expressed as mean ± SEM (n = 3). *** $p < 0.001$, ** $p < 0.01$, * $p < 0.05$. **(b)** Tumor progression curves in athymic NCI-nu/nu mice challenged subcutaneously with 2×10^6 Hec50co cells in the right flank. Mice were treated

with either saline (naïve), 5 mg/kg PTX**s**, 5 mg/kg PTX**p** (75/T), or the combination therapy of 5 mg/kg PTX**p** (75/T) and 5 mg/kg BIBF**p** (75/T). Treatments were administered IV through retro-orbital injections in the venous sinus on days 18, 25, and 32. Statistical analysis was performed using a non-parametric Kruskal- Wallis test. Data are presented as mean ± SEM (n = 7 for combination group, otherwise, n = 5). * $p < 0.05$, *** $p < 0.001$. **(c)** Representative photographs of tumors (black dotted circles) on day 32 post tumor challenge. **(d)** Kaplan-Meier survival curves comparing variously treated mice with the naïve group. Values of median survival is shown in brackets. Statistical analysis was performed using the Log-rank test with Bonferroni post hoc test. * $p < 0.05$ compared to the naïve group. **(e)** Mice weight change over time during treatments. Mice were weighted on days 18, 25 and 32. Data are presented as mean ± SEM. **(f)** H & E staining of mice organs collected after euthanizing the treated mice (mice were treated as described in (**b**)). Mice were euthanized when their tumor dimensions reached 2 cm in length or width, or 1 cm in height. Images were captured using 100x lens. Scale bar = 40 μm. **(g)** Intra-tumoral PTX concentration over a 12 h period following single IV (retro-orbital) injection of either 5 mg/kg PTX**s** or 5 mg/kg PTX**p** (75/T) quantified using a validated LC-MS/MS method (see Supplementary Methods). Statistical analysis was performed using unpaired two-tailed t-test. Data are expressed as mean ± SEM (n = 3). ** $p < 0.01$.

Table 1

Characterization of Blankp and PTXp prepared using different PLGA grades and different surfactants as well as BIBFp (75/T).

Formula abbreviation	Particle size (d.nm)	PDI	Zeta potential (mV)	Encapsulation efficiency (%)	Drug loading (μg drug/mg nanoparticles)
Blankp (75/T)	136.7±2.2	0.06±0.04	−47.9±2.0	–	–
Blankp (75/P)	173.6±3.8	0.05±0.04	−40.2±4.0	–	–
Blankp (50/T)	138.0±4.3	0.06±0.03	−48.4±5.7	–	–
Blankp (50/P)	167.3±3.1	0.04±0.01	−34.2±0.6	–	–
PTXp (75/T)	140.7±4.0	0.18±0.10	−47.2±3.2	56.4±3.7	47.0±3.1
PTXp (75/P)	163.1±4.9	0.11±0.05	−40.1±5.8	31.6±3.2	26.3±2.7
PTXp (50/T)	143.1±7.2	0.09±0.02	−52.2±5.5	38.9±2.9	32.4±2.4
PTXp (50/P)	147.8±10.5	0.07±0.06	−41.7±6.2	25.0±0.9	20.8±0.8
BIBFp (75/T)	109.5±15.1	0.09±0.01	−42.8±5.4	49.7±8.3	41.4±6.9

Data are presented as mean±SD (n=3).

75=PLGA (75:25), 50=PLGA (50:50), T=TPGS, P=PVA